American Mineralogist, Volume 85, pages 436–448, 2000

Crystal chemistry of Al-rich biotites coexisting with muscovites in peraluminous granites

MARIA FRANCA BRIGATTI,[1,*] PAOLA FRIGIERI,[1] CLAUDIO GHEZZO,[2] AND LUCIANO POPPI[1]

[1]Dipartimento di Scienze della Terra, Università di Modena e Reggio Emilia, Italy
[2]Dipartimento di Scienze della Terra, Università di Siena, Italy

ABSTRACT

A comparison was made between single-crystal structure refinements, electron microprobe analyses and octahedral site populations of seven biotite crystals and data obtained previously for coexisting muscovite in peraluminous granites using the same methods. Both micas, from several plutons of Northern Victoria Land (Antarctica) and Sardinia (Italy), show significant octahedral substitutions: biotite has a composition characterized by relatively high $^{[6]}$Al content ($0.32 \leq {}^{[6]}\text{Al} \leq 0.59$ apfu), whereas muscovite is characterized by phengite-like substitutions [$0.12 \leq {}^{[6]}(\text{Mg} + \text{Fe} + \text{Ti} + \text{Mn}) \leq 0.35$]. Mean bond-lengths and electron count data for six biotites-1*M* (space group *C*2/*m,* agreement factor $2.7\% \leq R_{obs} \leq 3.6\%$) and a biotite-2$M_1$ (space group *C*2/*c*, $R_{obs} = 2.8\%$) show that Al substitutes for divalent cations in the octahedral M2 site and that the Fe and Mg distribution is disordered. The mean tetrahedral bond lengths determined for biotite-2M_1 reflect Al-Si disorder. In coexisting muscovite-2M_1 crystals, small positive electron density residuals close to M1 site position as well as the increase in M2 mean atomic number is in agreement with the presence of a significant phengitic component. Reduction in biotite unit-cell dimensions with the increase of Al follows a pattern similar to that of associated muscovites, and the octahedral site volumes of both micas are influenced by the Al saturation index (ASI) of the rock. These results, and the calculated partition coefficients between biotite and muscovite for elements in M sites, are consistent with continuous reaction and re-equilibration of biotite and muscovite during crystallization of peraluminous granitic melts.

INTRODUCTION

Two-mica, strongly peraluminous granites are considered the product of ultrametamorphism leading to anatexis of aluminous metasedimentary rocks in the continental crust (Miller et al. 1981; White and Chappell 1983; Miller 1985; Neiva et al. 1987; Pitcher 1988, Patiño Douce and Johnston 1991). It is generally accepted that micas play an important role in the anatexis of aluminous metasediments and in the evolution of peraluminous granitic suites, and that the partition coefficients of major and trace elements between biotite and muscovite are a key to understanding the thermodynamic relationships and detailed kinetics of the process (De Albuquerque 1975; Tracy 1978; Speer 1984; Monier and Robert 1986; Patiño Douce and Johnston 1991). Knowledge of the chemistry of these phases therefore enables one to obtain barometric and thermometric information (Guidotti et al. 1989; Hoisch 1989; Patiño Douce et al. 1993; Guidotti et al. 1994). In an experimental study carried out at constant H_2O pressure and in the temperature range 600–750 °C, Icenhower and London (1995) suggest that: (1) biotite is stable over the complete temperature range, whereas muscovite stability is limited to about 715 °C; (2) at higher temperatures, dioctahedral mica displays high Fe and Ti content, which accounts for solid solutions with trioctahedral micas; (3) biotite reacts continuously with the melt, such that its Ti, Ba, and $^{[4]}$Al content increases in direct proportion to the rise in temperature; (4) there is no evidence of $^{[6]}$Al systematic variation with the Al saturation index of the melt.

In view of this, it is surprising that the structural relations between coexisting muscovite and biotite have attracted relatively little attention, because knowledge of the site geometric variations and of the cation partitioning can help in defining the thermodynamic and compositional parameters in force during the petrological and geochemical processes involved in the differentiation of such granites. The present study compares the crystal structure and site occupancy of biotites-1*M* and biotites-2M_1 coexisting with igneous muscovites-2M_1 in peraluminous granite plutons.

OCCURRENCE OF MICAS

The mica crystals occur in different peraluminous granitic rocks (Table 1). They were selected in granodioritic to monzogranitic cordierite-bearing plutons outcropping in Northern Victoria Land, Antarctica, and in Sardinia Island, Italy (Di Vincenzo et al. 1994; Biagini et al. 1991). In these samples muscovite coexists with biotite and can be considered of igneous origin on the basis of textural and microscopic criteria (Miller et al. 1981).

The Northern Victoria Land samples are from a wide belt of stocks and plutons of Cambro-Ordovician postkinematic

*E-mail: brigatti@unimo.it

0003-004X/00/0304–436$05.00

TABLE 1. Bulk rock composition (major oxides wt%) of peraluminous granites from Sardinia (Italy) and Northern Victoria Land (Antarctica)

	Sardinia			Antartica			
	A4	GFS15a	H87	CC1	C3-31	B1	C6c
SiO_2	72.43	72.50	76.27	73.65	71.19	72.81	73.15
TiO_2	0.29	0.26	0.01	0.22	0.42	0.34	0.18
Al_2O_3	14.20	14.71	13.5	14.29	14.93	14.22	14.57
Fe_2O_3	0.01	0.00	0.17	0.00	0.77	0.51	0.19
FeO	2.29	1.70	0.70	1.18	1.55	1.53	0.97
MnO	0.04	0.04	0.06	0.09	0.06	0.10	0.03
MgO	0.68	0.49	0.02	0.43	0.53	0.59	0.34
CaO	1.66	1.11	0.25	1.12	1.55	1.16	1.13
Na_2O	3.10	3.08	4.32	3.30	2.61	2.61	2.50
K_2O	4.37	4.97	4.18	5.08	5.33	5.48	6.16
P_2O_5	0.24	0.25	0.02	0.15	0.15	0.17	0.07
L.O.I.	0.69	0.89	0.5	0.49	0.90	0.47	0.71
A.S.I	1.26	1.24	1.12	1.13	1.19	1.19	1.14

Note: Al saturation index (A.S.I.) = the molecular ratio Al_2O_3 / (K_2O + Na_2O + CaO).

peraluminous granitoids related to the Ross Orogen and occurring between Priestley and Aviator Glaciers: three samples (29.01.88 C6C = C6c; 31.01.88 C3 = C3-31; and 28.12.90 B1 = B1) were collected around the Tinker Glacier, whereas sample 31.12.90 CC1 = CC1 is from the Frontier Mountains area. The Tinker type granites, showing biotite ± muscovite ± garnet ± cordierite as characteristic phases, are medium grained granodiorites and monzogranites with metasedimentary sillimanite-rich inclusions, whereas Frontier Mountain granites are characterized only by biotite ± muscovite. Ilmenite and graphite were found as accessory phases in all samples. The few barometric estimates reported by Biagini et al. (1991) are in line with a crystallization pressure of about 400 MPa.

The Sardinia samples are from two different peraluminous intrusions belonging to the Hercynian Sardinia-Corsica Batholith. Two samples (A4 and GFS15a) are from Sos Canales pluton (Central Sardinia), whereas sample H87 is from Riu Morunzu two-mica leucogranite (North Eastern-Sardinia). On the basis of mineral phase distribution and extent, the Sos Canales pluton, characterized by quartz, potassium feldspar, plagioclase, biotite, muscovite, andalusite, cordierite, and ilmenite, can be subdivided into two main units, namely, two-mica monzogranite (sample GFS15a) and granodiorite (sample A4) (Di Vincenzo et al. 1994). The pressure is estimated as 300–400 MPa (Di Vincenzo et al. 1994). The Riu Morunzu pluton (1–2 km large, estimated pressure less than 300 MPa) consists of a medium grained leucocratic alkali feldspar granite characterized by quartz, potassium feldspar, albite, muscovite, and low amount of biotite; garnet is only present in the late fine-grained differentiated dikes (Di Vincenzo et al. 1996).

EXPERIMENTAL METHODS

Chemical analyses

Major element analyses of micas were carried out on a wavelength-dispersive ARL-SEMQ electron microprobe (operating conditions: 15 kV accelerating voltage, 15 nA sample current and defocused electron beam with about 3 μm spot size). Minerals were used as standards, and analyses of secondary standards were performed to verify the analysis procedure. Analyses and data reductions were performed using the Probe software package of Donovan (1995). Fluorine determination was obtained following the procedure of Foley (1989). The overlap of Ti$K\alpha$ and Ba$L\alpha$ peaks was accounted for when obtaining Ti and Ba contents.

Chemical analyses of several mica crystals were first carried out on polished thin sections. A large number of mica crystals were analyzed in each section and multiple-point analyses were performed for each crystal to test its chemical homogeneity. The intragranular compositional variation of the individual crystal was, for major elements, within 3% of the estimated instrumental error, indicating a high degree of chemical homogeneity within each crystal. Individual point analyses for each crystal were averaged.

The chemical formulas were obtained using two calculation schemes.

Scheme 1. Because electron microprobe data cannot provide the oxidation state of Fe or contents of all volatile species, and also to compare the substitution mechanisms in our micas with those previously reported, chemical formulas were calculated using the following normalization procedure: (1) the positive charges were balanced to 10 O atoms and (OH + F + Cl) = 2; (2) all Fe was assumed to be Fe^{2+}; (3) the tetrahedral sites were filled with Si and Al to an occupancy of exactly 4; (4) the remaining Al was assigned to octahedral sites together with divalent cations (excluding Ca and Ba) and Ti; 5) the interlayer sites were filled with Na, K, Ca, and Ba. The results of these calculations are reported in Table 2[1] and Figures 1–3.

Scheme 2. For crystals used in the structure refinements, the chemical compositions reported in Table 3 were obtained by combining the results of (1) microprobe chemical analyses carried out on the same crystal as was used for the structure refinement, an average of at least six spots for each single plate being reported and (2) $(OH)^-$ determinations on several crystals from the same sample that yielded the crystal used for the structure refinement. Weight loss was determined by thermogravimetric analysis in a flow of Ar gas to minimize the reaction $2FeO + 2(OH)^- \rightarrow Fe_2O_3 + H_2 + O^{2-}$ using a Seiko SSC

[1]For a copy of Table 2, document item AM-00-040, contact the Business Office of the Mineralogical Society of America (see inside front cover of recent issue) for price information. Deposit items may also be available on the American Mineralogist web site (http://www.minsocam.org).

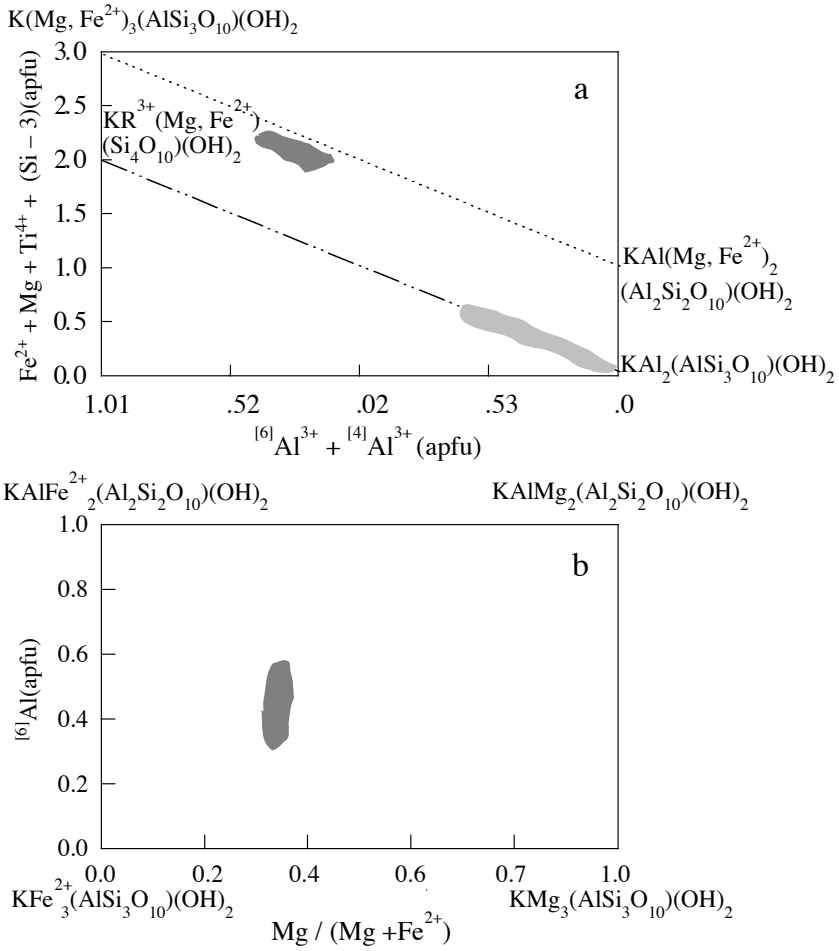

FIGURE 1. (**a**) Plot of $[Fe^{2+} + Mg + Ti + (Si–3)]$ (apfu) vs. total Al (apfu); (**b**) The ideal biotite plane (Guidotti 1984). Chemical formulas are based on $O_{10}(OH)_2$ negative charges. $R^{3+} = Fe^{3+} + Al$. Dark gray areas = biotite; light gray area = muscovite.

5200 thermal analyzer (heating rate of 10 °C/min; flow rate of 200 mL/min). The determination was based on the weight loss observed in the temperature range 750–1200 °C and adjusted to account for the mean F and Cl content determined by microprobe analysis; (3) Fe^{2+} determination by a semi-microvolumetric method (Meyrowitz 1970). The chemical formulas were based on $O_{12-x-y-z}(OH)_xF_yCl_z$ where x is OH pfu, y is F pfu, and z is Cl pfu.

Single-crystal X-ray diffraction and structure refinement

Single-crystal precession photographs were taken for several biotite crystals selected from the same crushed rock sample. In addition to the most common disordered stacking sequences, the ordered 1*M* polytype was found in samples A4, GFS15a, H87, CC1, C3-31, and B1, whereas the ordered $2M_1$ polytype was found only in sample C6c. $2M_1$ and 3*T* sequences with relevant spot streaking were identified in sample CC1.

To determine cell dimension and collect intensity data, the best crystal of each sample was mounted onto a Siemens P4P rotating-anode single crystal diffractometer, using graphite-monochromatized Mo*K*α radiation (operating conditions: 52 kV and 140 mA) and equipped with XSCANS software (Siemens 1996). Unit-cell parameters (Table 4) were calculated from least-squares refinement of nearly 50 medium-high angle reflections in the range $15 \le 2\theta \le 25°$.

Reflections ($\pm h, \pm k, l$) were collected in the range $4.0° \le 2\theta \le 70.0°$ using ω scan, with a window width of 1.4° to 3.4° and variable reflection scanning speeds. The intensities and positions of three standard reflections were checked every 100 reflections to monitor crystal and electronic stability. The intensities were corrected for Lorentz-polarization effects and for absorption using a calibration curve obtained by the ψ scan method. The symmetrically equivalent reflection intensities were averaged and the resulting discrepancy factors ($R_{sym} = \Sigma_{hkl} \Sigma_{i=1}^{N} |I_{hkl_i} - \bar{I}_{hkl_i}| / \Sigma_{hkl} \Sigma_{i=1}^{N} \bar{I}_{hkl_i}$) calculated to be in the range $1.6 \le R_{sym} \le 3.5\%$. The crystal structure refinements were performed in the space groups *C*2/*m* and *C*2/*c*, for 1*M* and $2M_1$ polytypes, respectively, (program ORFLS, Busing et al. 1962) on selected ($I \ge 5\sigma_I$) reflections (Ungaretti 1980, Ungaretti et al. 1983). No weights and no constraints were used, and the residuals (R_{obs}) obtained at the end of the least-squares refinements were A4 = 3.2%; GFS15a = 3.6%; H87 = 3.2%; CC1 = 3.2%; C3-31 = 3.1%; B1 = 2.7%; C6c = 2.8%. Atomic position parameters for biotites 1*M* and $2M_1$, respectively, reported by Bigi and Brigatti (1994), were used as initial values for all refinements. Appropriate fully ionized scattering factors were applied to octahedral M1 and M2 and interlayer A sites, whereas mixed scattering factors were assumed for anion (O vs. O^{2-}) and tetrahedral sites

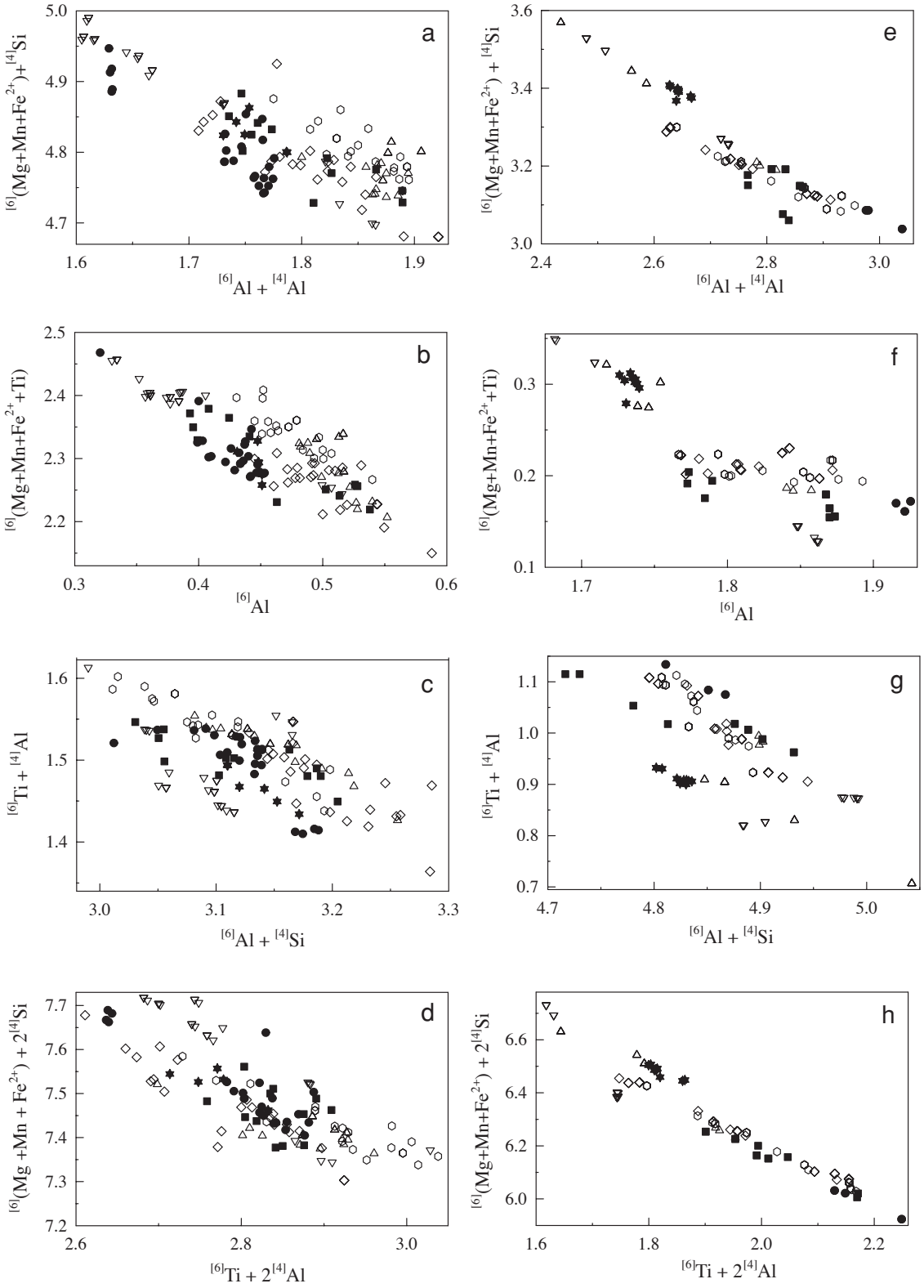

FIGURE 2. Biotite (**a**, **b**, **c**, and **d** plot) and muscovite (**e**, **f**, **g**, and **h** plot) chemical variations in peraluminous granites. The atoms per formula unit (apfu) of each chemical element were combined to obtain the exchange vectors in Equations 1, 2, 3, and 4 (see text). Chemical formulas are based on $O_{10}(OH)_2$ negative charges. Filled symbols: Sardinia samples (circle = A4, square = GFS15a, star = H87); open symbols: Northern Victoria Land samples (diamond = CC1, triangle down = C3-31, hexagon = B1, triangle up = C6c).

TABLE 3. Averaged chemical composition and structural formulas for biotite crystals

	Sardinia			Antartica			
	A4	GFS15a	H87	CC1	C3-31	B1	C6c
			Chemical composition (oxides wt%)				
SiO_2	34.97	34.85	35.03	34.81	33.64	33.76	35.16
TiO_2	3.67	2.42	2.75	2.99	3.42	2.91	2.69
Al_2O_3	17.96	21.08	19.34	21.64	20.11	21.09	20.86
Fe_2O_3	0.16	–	–	–	–	0.17	–
FeO	22.41	21.09	22.48	20.67	22.68	21.71	21.19
MgO	6.70	6.35	6.04	6.42	5.99	7.16	6.15
MnO	0.54	0.32	0.47	0.54	0.91	0.48	0.61
CaO	b.d.t.	0.31	b.d.t.	b.d.t.	0.11	0.09	0.07
BaO	b.d.t.	0.18	b.d.t.	b.d.t.	0.18	b.d.t.	b.d.t.
Na_2O	0.24	0.11	0.11	0.07	0.18	0.19	0.11
K_2O	9.65	9.76	9.91	9.80	9.66	9.44	9.96
H_2O	3.49	3.06	3.03	3.04	3.08	2.99	3.20
F	0.20	0.49	0.62	b.d.t.	0.04	b.d.t.	b.d.t.
Cl	b.d.t.	b.d.t.	0.21	b.d.t.	b.d.t.	b.d.t.	b.d.t.
Sum	99.99	100.02	99.99	99.98	100.00	99.99	100.00
			Structural formulas (apfu) based on $O_{(12-x-y-z)}$ $(OH)_x$ F_y Cl_z				
Si	2.71	2.69	2.72	2.68	2.63	2.62	2.71
Al	1.29	1.31	1.28	1.32	1.37	1.38	1.29
Sum	4.00	4.00	4.00	4.00	4.00	4.00	4.00
Ti	0.21	0.14	0.16	0.17	0.20	0.17	0.16
Fe^{3+}	0.01	–	–	–	–	0.01	–
Fe^{2+}	1.45	1.36	1.46	1.33	1.48	1.41	1.36
Mg	0.77	0.73	0.70	0.73	0.70	0.83	0.71
Mn	0.04	0.02	0.03	0.04	0.06	0.03	0.04
Al	0.35	0.60	0.50	0.64	0.48	0.54	0.60
Sum	2.83	2.85	2.85	2.91	2.92	2.99	2.87
Na	0.04	0.02	0.02	0.01	0.03	0.03	0.02
K	0.95	0.96	0.98	0.96	0.96	0.93	0.98
Ca	–	0.03	–	–	0.01	0.01	0.01
Ba	–	0.01	–	–	0.01	–	–
Sum	0.99	1.02	1.00	0.97	1.01	0.97	1.01
OH	1.80	1.57	1.57	1.56	1.61	1.54	1.64
F	0.05	0.12	0.15	–	0.01	–	–
Cl	–	–	0.03	–	–	–	–
O	10.15	10.31	10.25	10.44	10.38	10.46	10.36
Sum	12.00	12.00	12.00	12.00	12.00	12.00	12.00

Note: b.d.t. = below detection threshold.

TABLE 4. Unit-cell parameters of biotite crystals

	Sardinia			Antartica			
	A4	GFS15a	H87	CC1	C3-31	B1	C6c
a (Å)	5.352(1)	5.339(1)	5.344(3)	5.328(1)	5.347(2)	5.336(1)	5.335(1)
b (Å)	9.268(3)	9.232(2)	9.256(3)	9.222(2)	9.257(1)	9.239(2)	9.242(2)
c (Å)	10.255(3)	10.208(2)	10.237(2)	10.197(2)	10.211(1)	10.200(2)	20.181(4)
β (°)	100.27(2)	100.30(2)	100.27(3)	100.26(1)	100.27(2)	100.29(2)	95.20(2)
V (Å^3)	500.5(3)	495.1(1)	498.2(3)	493.0(2)	497.3(2)	494.8(2)	991.0(3)
Polytype	1*M*	1*M*	1*M*	1*M*	1*M*	1*M*	$2M_1$

Note: Values in parentheses represent estimated standard deviations.

(75Si–25Al vs. $75Si^{4+}$–$25Al^{3+}$).

At the final stage of the refinement, a complete Fourier difference electron density (DED) map was calculated. On the DED map, some crystals reveal an electron density excess above background (≥3σ) close to the H position [x = 0.098(2), y = 0.500 Å, z = 0.3007(8) Å], as suggested by the neutron diffraction study of phlogopite-1*M* reported by Joswig (1972) (A4-1*M*: x = 0.092 Å, y = 0.503 Å, z = 0.314 Å; GFS15a-1*M*: x = 0.158 Å, y = 0.502 Å, z = 0.332 Å; C3-31-1*M*: x = 0.013 Å, y = 0.501 Å, z = 0.299 Å; CC1-1*M*: x = 0.129 Å, y = 0.504 Å, z = 0.323 Å), whereas in the C6C-$2M_1$ polytype there is a peak (3σ above background) at x = 0.946 Å, y = 0.084 Å, z = 0.105 Å with a distance of 1.0 Å from O4. No attempts were made to introduce the coordinates of the atom located in each refinement. Table 5[1] summarizes crystallographic coordinates and isotropic and anisotropic temperature factors, while relevant bond lengths are listed in Table 6 and Table 7 for 1*M* and $2M_1$ crystals, respectively. Observed and calculated structure factors are shown in Table 8[1]. Selected tetrahedral, octahedral and interlayer parameters are reported in Table 9.

[1]For a copy of Tables 5 and 8, document item AM-00-040, contact the Business Office of the Mineralogical Society of America (see inside front cover of recent issue) for price information. Deposit items may also be available on the American Mineralogist web site (http://www.minsocam.org).

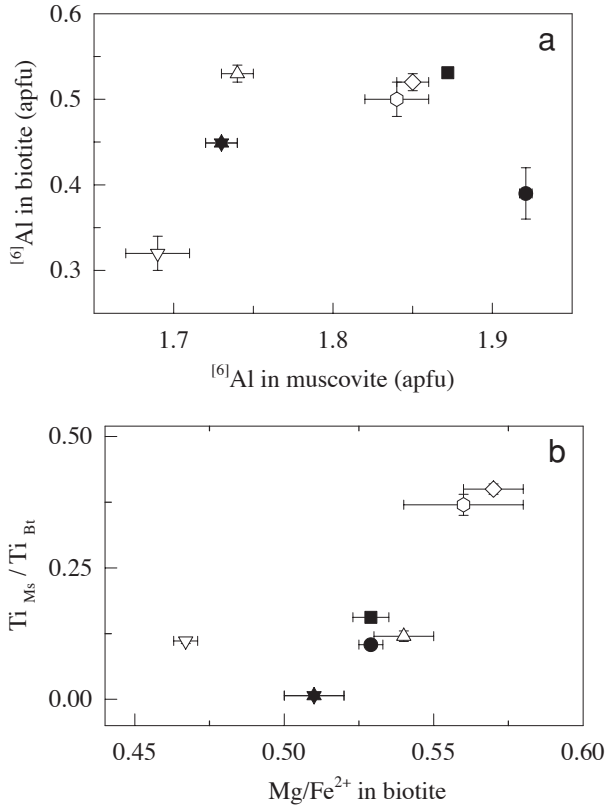

FIGURE 3. (**a**) The mean $^{[6]}$Al (apfu) content in muscovite plotted against the mean $^{[6]}$Al (apfu) of coexisting biotite crystals; (**b**) Plot of the ratio between the mean Ti content in muscovite and those in coexisting biotite crystals (Ti_{Ms}/Ti_{Bt}) vs. the mean Mg/Fe^{2+} ratio in biotite (after Guidotti et al. 1977). Formulas and symbols are as in Figure 2.

TABLE 6. Selected bond lengths (Å) from structure refinements of biotite-1*M* crystals

	Sardinia			Antartica		
	A4	GFS15a	H87	CC1	C3-31	B1
Tetrahedral bond lengths						
T-O1	1.665(2)	1.656(2)	1.659(1)	1.653(2)	1.658(1)	1.654(1)
T-O2	1.660(3)	1.663(2)	1.662(2)	1.659(2)	1.660(2)	1.659(2)
T-O2'	1.665(3)	1.648(3)	1.656(2)	1.652(2)	1.659(2)	1.650(2)
T-O3	1.670(2)	1.663(2)	1.674(2)	1.662(2)	1.665(2)	1.668(2)
<T-O>	1.665	1.658	1.663	1.657	1.660	1.658
Octahedral bond lengths						
M1-O3 (×4)	2.112(2)	2.100(2)	2.109(2)	2.103(2)	2.108(2)	2.103(2)
M1-O4 (×2)	2.080(3)	2.073(3)	2.085(3)	2.074(3)	2.076(3)	2.076(2)
<M1-O>	2.101	2.091	2.101	2.093	2.097	2.094
M2-O3 (×2)	2.084(2)	2.074(2)	2.076(2)	2.068(2)	2.081(2)	2.075(2)
M2-O3' (×2)	2.080(3)	2.073(2)	2.072(2)	2.068(2)	2.078(2)	2.070(1)
M2-O4 (×2)	2.056(2)	2.053(2)	2.051(2)	2.039(2)	2.050(2)	2.042(2)
<M2-O>	2.073	2.067	2.066	2.058	2.070	2.062
Interlayer cation bond lengths						
A-O1 (×2)	2.981(4)	2.982(4)	2.989(3)	2.979(3)	2.996(3)	2.986(2)
A-O1' (×2)	3.386(4)	3.360(4)	3.368(3)	3.363(4)	3.354(3)	3.356(2)
A-O2 (×4)	2.987(3)	2.997(2)	2.989(2)	2.977(2)	2.992(2)	2.993(2)
A-O2' (×4)	3.367(3)	3.330(3)	3.352(2)	3.340(3)	3.335(2)	3.327(2)
A-O4 (×2)	4.008(2)	3.986(4)	3.999(3)	3.991(3)	3.994(3)	3.993(2)

Note: Values in parentheses represent estimated standard deviations.

TABLE 7. Selected bond lengths (Å) from structure refinements of biotite-2*M*$_1$ crystal (sample C6c)

Tetrahedral sheet		Octahedral sheet		Interlayer sheet	
T1-O11	1.660(2)	M2-O31	2.025(2)	A-O11 (×2)	2.989(2)
T1-O21	1.658(2)	M2-O31'	2.120(2)	A-O11' (×2)	3.362(2)
T1-O22	1.654(2)	M2-O32	2.116(2)	A-O21 (×2)	2.987(2)
T1-O31	1.666(2)	M2-O32'	2.075(2)	A-O21' (×2)	3.341(2)
<T1-O>	1.660	M2-O4	1.995(2)	A-O22 (×2)	2.989(2)
T2-O11	1.650(2)	M2-O4'	2.046(2)	A-O22' (×2)	3.335(2)
T2-O21	1.654(2)	<M2-O>	2.063	A-O4 (×2)	3.998(2)
T2-O22	1.661(2)	M1-O31 (×2)	2.111(2)		
T2-O32	1.665(2)	M1-O32 (×2)	2.061(2)		
<T2-O>	1.658	M1-O4 (×2)	2.126(2)		
		<M1-O>	2.099		

Note: Values in parentheses represent estimated standard deviations.

The average effective radius of the cations occupying individual octahedral sites, in addition to site-scattering refinement, provides constraints on the occupancy of octahedral sites. Thus, the M1 and M2 site occupancy was calculated by combining, in a system of equations, the results of both microprobe analyses and single-crystal X-ray refinement (i.e., <M1-O> and <M2-O> mean bond distances and mean electron counts at M1 and M2 sites), taking into account the charge-balance requirements. The best fraction x_i for each species was determined by identifying the vector which best fits an overdetermined equation system $\mathbf{A}\boldsymbol{x} = \mathbf{b}$, where $\mathbf{A}$ is the matrix of coefficients ($n \times m$), $\mathbf{b}$ is the vector of known terms and $\boldsymbol{x}$ is the vector of the unknown. Namely $\mathbf{A} = \{a_{ij}\}$, $\boldsymbol{x} = \{x_i\}$ and $\mathbf{b} = \{b_i\}$, the coefficient a_{ij}, represents the influence of species j over the balance expressed by equation number i. To find the vector which best fits the system, a least-squares method was used, calculating the minimum for the function $F(x) = \mathbf{R^T}*\mathbf{R}$, where $\mathbf{R} = \mathbf{A}*\boldsymbol{x}-\mathbf{b}$. The accuracy of the fit between observed and calculated values was evaluated by the Q parameter:

$$\left[Q = \sum_{i=1}^{n} \left(b_i - \sum_{j=1}^{m} \left(a_{ij} x_j \right) \right)^2 \right].$$

The ideal <M-O> mean bond distances for Fe^{2+}, Fe^{3+}, Mn, Ti were those calculated for each species by Weiss et al. (1985); for the <Mg-O> distance the value of a synthetic phlogopite refined by Hazen and Burnham (1973) and for <Al-O> the value reported by Guggenheim et al. (1987) for Panasqueira muscovite crystal were used, whereas for vacancy the mean <M1-O> distance found for the less phengitic muscovites (Brigatti et al. 1998a) was used. To reduce the variables, M2 sites were considered completely filled, any vacancies being assigned to the M1 site; Mn was added to Fe^{2+}, Ti was considered ordered at the M2 site. The site populations which best fit the observed chemical and structural data, giving Q values in the range $2.3 \cdot 10^{-4}$–$5.4 \cdot 10^{-4}$, are in Table 10.

RESULTS AND DISCUSSION

Chemistry

Biotite compositions cover the fields between $1.61 \le (^{[4]}\text{Al} + ^{[6]}\text{Al}) \le 1.93$ apfu and $1.81 \le \text{Fe}^{2+} + \text{Mg} + \text{Ti} + (\text{Si}-3) \le 2.20$ apfu, whereas muscovite compositions cover the fields between $2.43 \le (^{[4]}\text{Al} + ^{[6]}\text{Al}) \le 3.04$ apfu and $0.04 \le \text{Fe} + \text{Mg} + \text{Ti} + (\text{Si}-3) \le 0.58$ apfu (Fig. 1a). The deviation of biotite from the ideal solid solution $K(Fe,Mg)_3AlSi_3O_{10}(OH)_2$-$K(Fe,Mg)_2$

TABLE 9. Selected parameters derived from structure refinements of biotite-1*M* and biotite-2M_1 crystals

	Sardinia			Antartica			
Sample	A4	GFS15a	H87	CC1	C3-31	B1	C6c
Polytype	1*M*	1*M*	1*M*	1*M*	1*M*	1*M*	2M_1
				Tetrahedral parameters			
α (°)	8.50	7.65	8.07	8.12	7.61	7.59	7.85
Δz(Å)	0.0114	0.0081	0.0154	0.0021	0.0180	0.0187	0.0237
τ_{T1} (°)	110.1	110.2	110.1	110.2	110.2	110.1	110.1
τ_{T2} (°)							110.2
TAV_{T1} (°)^2	0.5	0.8	0.5	0.6	0.6	0.5	1.9
TAV_{T2} (°)^2							1.8
TQE_{T1} (Å)	1.0001	1.0002	1.0002	1.0002	1.0002	1.0002	1.0005
TQE_{T2} (Å)							1.0005
$Volume_{T1}$ (Å^3)	2.37	2.34	2.36	2.33	2.35	2.34	2.34
$Volume_{T2}$ (Å^3)							2.33
BLD_{T1} (%)	0.149	0.318	0.337	0.248	0.149	0.344	0.197
BLD_{T2} (%)							0.345
ELD_{T1} (%)	0.476	0.573	0.611	0.560	0.543	0.585	0.818
ELD_{T2} (%)							0.667
				Interlayer cation parameters			
<A-O>$_{inner}$(Å)	2.985	2.992	2.989	2.978	2.993	2.991	2.988
<A-O>$_{outer}$(Å)	3.373	3.340	3.357	3.348	3.341	3.337	3.346
Δ<A-O>(Å)	0.388	0.348	0.368	0.370	0.348	0.346	0.358
				Octahedral parameters			
ψ_{M1} (°)	59.26	59.27	59.42	59.46	59.30	59.36	59.44
ψ_{M2} (°)	58.80	58.87	58.84	58.88	58.86	58.91	58.84
$E_{s\,M1}$ (Å)	2.806	2.792	2.801	2.788	2.799	2.791	2.799
$E_{s\,M2}$ (Å)	2.786	2.774	2.775	2.762	2.778	2.767	2.772
$E_{u\,M1}$ (Å)	3.128	3.114	3.133	3.123	3.124	3.123	3.130
E_{uM2} (Å)	3.071	3.064	3.062	3.052	3.068	3.059	3.057
OQE_{M1}	1.0130	1.0131	1.0139	1.0142	1.0134	1.0140	1.0142
OQE_{M2}	1.0105	1.0108	1.0107	1.0110	1.0109	1.0112	1.0121
OAV_{M1} (°)	42.1	42.6	45.0	46.0	43.4	45.6	54.2
OAV_{M2} (°)	34.8	35.8	35.4	36.4	35.8	36.7	37.3
$Vol._{M1}$ (Å^3)	12.13	11.96	12.12	11.97	12.06	12.00	12.08
$Vol._{M2}$(Å^3)	11.70	11.58	11.58	11.43	11.63	11.51	11.51
BLD_{M1} (%)	0.684	0.591	0.500	0.613	0.674	0.573	1.224
BLD_{M2} (%)	0.561	0.444	0.484	0.628	0.638	0.650	1.980
ELD_{M1} (%)	5.339	5.442	5.594	5.659	5.489	5.620	5.566
				Sheet thickness			
Tetr. (Å)	2.259	2.251	2.260	2.252	2.258	2.256	2.254
Oct. (Å)	2.148	2.137	2.138	2.127	2.141	2.130	2.135
Inter. (Å)	3.424	3.404	3.414	3.403	3.390	3.394	3.406
Δ_{TM} (Å)	0.537	0.521	0.533	0.537	0.522	0.527	0.525

Notes: α (tetrahedral rotation angle) = $\Sigma_{i=1}^{6}\alpha_i/6$ where $\alpha_i = |120° - \phi_i|/2$ and where ϕ_i is the angle between basal edges of neighboring tetrahedra articulated in the ring. $\Delta z = [Z_{(O_{basal})max} - Z_{(O_{basal})min}]$ [csinβ]. τ (tetrahedral flattening angle) = $\Sigma_{i=1}^{3}(O_{basal\grave{o}} - \hat{T} - O_{basal})_i/3$. TAV (tetrahedral angle variance) = $\Sigma_{i=1}^{3}(\theta i - 109.47)^2/5$ (Robinson et al. 1971).TQE (tetrahedral quadratic elongation) = $\Sigma_{i=1}^{4}(l_i/l_o)^2/4$ where l_o is the center to vertex distance for an undistorted tetrahedron whose volume is equal to that of the distorted tetrahedron with bond length l_i (Robinson et al. 1971). ψ (octahedral flattening angle) = cos^{-1}[octahedral thickness / (2<M-O>)] (Donnay et al. 1964). e_u, e_s .= mean lengths of unshared and shared edges, respectively (Toraya 1981). OQE (octahedral quadratic elongation) $\Sigma_{i=1}^{6}(l_i/l_o)^2/6$ where l_o is the center to vertex distance for an undistorted octahedron whose volume is equal to that of the distorted octahedron with bond length l_i (Robinson et al. 1971). OAV (octahedral angle variance) = $\Sigma_{i=1}^{12}(\theta_i - \square 90)^2/11$ (Robinson et al. 1971). BLD = (bond length distortion) $\frac{100}{n}\Sigma_{i=1}^{n}\frac{|(X-O)_i - (X-O)|}{(X-O)}$% where *n* is the number of bonds and (X-O) the central cation-oxygen length (Renner and Lehmann 1986). ELD = (edge length distortion) $\frac{100}{n}\Sigma_{i=1}^{n}\frac{|(O-O)_i - (O-O)|}{(O-O)}$% where *n* is the number of bonds and (O-O) the polyedron edge length (Renner and Lehmann 1986). Δ_{TM} (dimensional misfit) = 2 <O-O>$_{basal}$ – 3$\sqrt{2}$ (2<M2-O> + <M1-O>)/3 (Toraya 1981).

$AlAl_2Si_2O_{10}(OH)_2$ was ascribed by Tracy (1978) to unanalyzed elements. Moreover, the presence of exchange vectors, such as Ti-oxy $^{[6]}(Mg^{2+},Mn^{2+},Fe^{2+})_{-1}OH^{-}_{-2}$ $^{[6]}Ti^{4+}O^{2-}_{2}$ and/or Al-oxy $^{[6]}(Mg^{2+},Mn^{2+},Fe^{2+})_{-1}OH^{-}_{-1}{}^{[6]}Al^{3+}O^{-2}$, which are not considered in the formula calculation, could enhance this deviation. In the ideal plane of trioctahedral micas (Guidotti 1984), the crystals studied cover the compositional range between $0.31 \le Mg/(Mg + Fe^{2+}) \le 0.38$ and $0.32 \le {}^{[6]}Al \le 0.59$ apfu, and can therefore be considered Al-rich biotites (Fig. 1b). From a chemical viewpoint, if one ignores anionic substitutions and vacancies mostly affected by the unit formula calculation method, the plots of Figures 2a–2d indicate that the variation of Al content in the biotite octahedral sites could be charge balanced by the following exchange operators:

$$^{[6]}(Mg^{2+},Mn^{2+},Fe^{2+})_{-1}\ {}^{[4]}Si^{4+}_{-1}\ {}^{[6]}Al^{3+}{}^{[4]}Al^{3+} \quad (1)$$

$$^{[6]}(Mg^{2+},Mn^{2+},Fe^{2+})_{-1}\ {}^{[6]}Ti^{4+}_{-1}\ {}^{[6]}Al^{3+}_{2} \quad (2)$$

$$^{[6]}Ti^{4+}_{-1}\ {}^{[4]}Al^{3+}{}_{1}{}^{[6]}Al^{3+}{}^{[4]}Si^{4+} \quad (3)$$

$$^{[6]}(Mg^{2+},Mn^{2+},Fe^{2+})_{-1}\ {}^{[4]}Si^{4+}_{-2}\ {}^{[6]}Ti^{4+}\ {}^{[4]}Al^{3+}_{2} \quad (4)$$

TABLE 10. Refined and calculated site occupancy (epfu)

	Sardinia			Antartica			
	A4	GFS15a	H87	CC1	C3-31	B1	C6c
			M1 Octahedral site				
Fe^{2+}	0.70	0.66	0.68	0.62	0.64	0.58	0.66
Mg	0.12	0.17	0.16	0.26	0.26	0.40	0.19
Vacancy	0.17	0.16	0.15	0.10	0.09	0.02	0.14
$m.a.n._{(calc.)}$	19.6	19.2	19.6	19.2	19.8	19.9	19.4
$m.a.n._{(X\text{-}ref.)}$	19.6(1)	19.1(1)	19.6(1)	19.4(1)	19.9(1)	19.8(7)	19.4(1)
			M2 Octahedral site				
Fe^{2+}	0.40	0.36	0.40	0.37	0.45	0.43	0.37
Mg	0.32	0.28	0.27	0.23	0.22	0.22	0.26
Ti	0.11	0.07	0.08	0.08	0.10	0.08	0.08
Al	0.17	0.29	0.25	0.32	0.24	0.27	0.30
$m.a.n._{(calc.)}$	19.9	18.1	18.8	18.4	19.7	19.2	18.4
$m.a.n._{(X\text{-}ref.)}$	18.9(2)	18.2(2)	18.8(1)	18.5(2)	19.6(2)	19.2(1)	18.4(2)
$m.a.n.\ (M1+2M2)_{calc.}$	57.4	55.4	57.2	56.0	59.1	58.3	56.2
$m.a.n.\ (M1+2M2)_{X\text{-}ref.}$	57.4(4)	55.5(4)	57.2(4)	56.4(4)	59.1(4)	58.2(3)	56.2(4)
$m.a.n.\ (M1+2M2)_{EPMA}$	57.3	55.5	57.1	56.4	59.0	58.4	56.2
			Interlayer site				
$m.a.n.\ A_{X\text{-}ref.}$	18.2(6)	19.8(5)	18.6(5)	18.7(5)	19.4(5)	18.3(4)	19.2(6)
$m.a.n.\ A_{EPMA}$	18.5	19.6	18.8	18.4	19.3	18.2	19.0

Notes: Xref = X-ray refinement; EPMA = electron probe microanalysis; calc = calculated using EPMA and X-ref. results (see "Experimental methods" section); m.a.n. = mean atomic number. Values in parentheses represent estimated standard deviations.

As indicated by Patiño Douce et al. (1993) the systematic increase of biotite $^{[6]}$Al content is not completely matched by $^{[4]}$Al. Therefore, at least two independent linear components are required to account for the total Al content in this phase. Figure 2 does not show separate domains for the biotite crystals from Northern Victoria Land and Sardinia. The $^{[6]}$Al mean values are virtually constant for Northern Victoria Land [$^{[6]}$Al = 0.46(7) (apfu)] and Sardinia [$^{[6]}$Al = 0.44(3) (apfu)] biotite, whereas, for individual samples, the mean $^{[6]}$Al values differ significantly [B1 = 0.48(3); C3-31 = 0.38(6); C6C = 0.51(2); CC1 = 0.50(3); A4 = 0.43(3); GFS15a = 0.46(5); H87 = 0.45(1) apfu]. The chemistry of coexisting muscovite (Figs. 2e–2h) is characterized by variable levels of Mg, Fe and Ti as Al octahedral substitutions. The phengitic component evaluated as a percentage of the ratio $(Fe^{2+} + Fe^{3+} + Mg + Ti + Mn)/ (Fe^{2+} + Fe^{3+} + Mg + Ti + Mn + Al)$ ranges from 0.8 to 17.2% in Northern Victoria Land muscovite, and from 7.6 to 15.3% in Sardinia muscovite.

The mean composition of muscovite crystals next to biotite suggests that the majority of the samples follow the systematic behavior first outlined by Tracy (1978), i.e., biotites with high Al content coexist with muscovite close to the ideal composition (Fig. 3a).

Patiño Douce and Johnston (1991) and Patiño Douce et al. (1993) carried out experimental studies on the vapor-absent melting behavior of a natural metapelitic rock in order to ascertain the mechanisms underlying the origin of peraluminous granitoids. They suggest that the solution of $^{[6]}$Al in biotite, modeled as a dioctahedral exchange component of the form Al_2Mg_{-3} or Al_2Fe_{-3}, largely depends both on pressure and temperature for biotite coexisting with garnet, aluminosilicates, and quartz. Additional information about melting reactions and the evolution of peraluminous granitic plutons can be obtained from the partition coefficients for the elements of interest in biotite and muscovite. Icenhower and London (1995), calculated the element partitioning among biotite, muscovite, and melt from an experimental study on H_2O-saturated peraluminous silicic melts at 200 MPa (H_2O). They found that the biotite/muscovite partition coefficients for Ti, Mg, and Fe are in the range: $D(Ti)^{Bt/Ms}$ = 3.3 (650 °C)–5.9 (700 °C); $D(Mg)^{Bt/Ms}$ = 3.5 (650 °C)–5.8 (700 °C); $D(Fe)^{Bt/Ms}$ = 4.5 (650 °C)–7.8 (700 °C).

The partition coefficients calculated here are in Table 11. To a first approximation, the $D(Ti)^{Bt/Ms}$ ($1.94 \le D(Ti)^{Bt/Ms} \le 3.33$) is almost identical to the partition coefficient of Ti for coexisting biotite and muscovite in silicic melt at 200 MPa H_2O (Icenhower and London 1995). In contrast, the Mg and Fe partition coefficients ($5.50 \le D(Mg)^{Bt/Ms} \le 82.59$; $5.23 \le D(Fe)^{Bt/Ms} \le 20.94$) are considerably larger. It is not surprising that differences exist between the experimentally derived partition coefficients and those obtained for natural systems. In simplified model systems the intensive variables and the exchange reactions are precisely defined, whereas in complex natural systems they are not. As observed by Patiño Douce (1993) the closer agreement between experimental and natural systems is for $D(Ti)^{Bt/Ms}$. The Ti content in biotite coexisting with iron-titanium oxide phases shows a non-linear increase with temperature, is sensitive to oxygen fugacity, and produces a stabilizing effect on this phase. The exchange components present in muscovite are the phengite substitutions ($^{[6]}Al^{3+}_{-1}\,^{[4]}Al^{3+}_{-1}\,^{[6]}(Mg^{2+}, Fe^{2+})^{[4]}Si^{4+}$) and the substitution of Ti coupled with Fe or Mg ($^{[6]}Al^{3+}_{-2}\,^{[6]}(Mg^{2+}, Fe^{2+})\,^{[6]}Ti^{4+}$). Guidotti (1978) demonstrated that as the

TABLE 11. Partitioning of elements ($^{[6]}$Al, Ti, Fe^{2+}, and Mg) between biotite and coexisting muscovite [$D(R^{n+})^{Bt/Ms}$]

	Sardinia			Antartica			
	A4	GFS15a	H87	CC1	C3-31	B1	C6c
$D(^{[6]}Al)^{Bt/Ms}$	0.22	0.25	0.26	0.28	0.21	0.26	0.29
$D(Ti)^{Bt/Ms}$	2.19	2.88	2.87	3.02	1.94	2.97	3.33
$D(Fe^{2+})^{Bt/Ms}$	17.27	20.94	5.23	17.97	14.29	17.58	12.55
$D(Mg)^{Bt/Ms}$	13.44	10.38	82.59	9.54	9.03	10.04	5.50

Note: For each sample D was calculated following Beattie et al. (1993) using the mean content of the element R^{n+} (apfu) from formulas based on 22 negative charges.

temperature increases the phengite component decreases, whereas the Ti component increases. The Ti content in the coexisting micas studied here seems to confirm the correlation of Guidotti et al. (1977) (Fig. 3b): there is a direct relationship between the ratio of Ti content in muscovite and biotite (Ti_{Ms}/Ti_{Bt}) and the Mg/Fe^{2+} ratio of coexisting biotite. By combining field and optical observations with chemical and partition coefficient results, it is reasonable to suggest crystallization temperatures around 650–700 °C for the granitoids studied, and an equilibrium crystallization for biotite and muscovite crystals.

Crystal structure and chemistry

Biotite 1M. Because one of our aims is to evaluate crystal chemical peculiarities of biotite from peraluminous granites, the crystal chemical relationships of biotite-1*M* from Northern Victoria Land and Sardinia granites are compared with those of biotite-1*M* crystals from plutonic complexes previously reported, namely, biotite crystals from Warburton granodiorite (Lachlan Fold Belt, Australia) and biotite crystals from Valle del Cervo plutonic complex (Northwestern Italy) (Brigatti and Davoli 1990; Bigi and Brigatti 1994; Brigatti et al. 1998b).

In the studied crystals, $^{[6]}$Al substitution ranges from 0.35 to 0.64 apfu (Table 3), decreases to zero in Valle del Cervo biotite crystals ($0.00 \le {}^{[6]}Al \le 0.05$ apfu) and ranges from 0.18 to 0.31 apfu in Warburton granodiorite. With respect to crystals of other plutons so far refined, biotites from peraluminous granites present similar M1 but smaller M2 site volumes (Fig. 4a). Comparison of individual M1-O and M2-O bond lengths shows that the shorter <M2-O> mean bond distances (i.e., the smaller M2 site volumes) primarily result from the difference in <M2-O3> bond lengths. These features may suggest that Al mostly occupies the M2 site. Figure 4b, where <M2-O3> mean bond distances are plotted against octahedral Al, confirms that M2 site size reduces as Al increase, whereas the relationships between octahedral sheet thickness and the $^{[6]}$Al content (Fig. 4c) suggest that the reduced dimensions of M2 involve a reduction of the whole sheet.

In all samples studied here, the site volumes, the distortion parameters and the mean electron counts of the trans M1 octahedral site are greater than those of the cis M2 site (Table 9). These results reflect the general trend of biotite octahedral ordering, which is mesoctahedral of type II (Weiss et al. 1992). Furthermore, in comparison with the previously studied crystals from plutonic suites, both octahedral sites are more distorted. Between M1 and M2, M1 shows the largest deviation from a perfect octahedron and M2 the smallest. The distortion of M1, as measured by the octahedral angle variance (OAV), increases as $^{[6]}$Al increases (Fig. 5a). The differences between M1 shared and unshared edge lengths, and consequently M1 distortion, correlate both with Fe/(Fe + Mg) and with Al contents (Figs. 5b and 5c). Therefore, M1 distortion appears to be controlled both by M1 and by M2 cation ordering: to satisfy the bond with M2, which has higher Al content, M1 reduces the length of the edges shared and extends that of unshared edges, thereby increasing distortion. In biotites-1*M* from peraluminous granites, the calculated site population for octahedral M1 and M2 indicate that Mg and Fe are distributed in both positions, whereas the M1 site is more Fe-rich. As a consequence of Fe increase, the M site

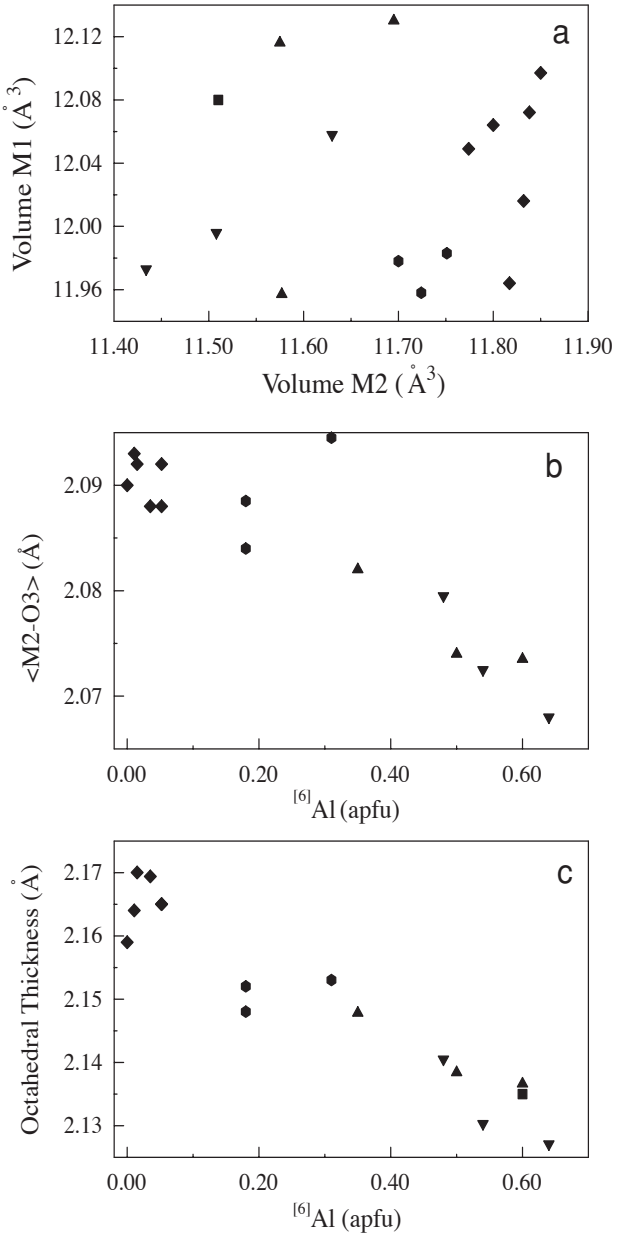

FIGURE 4. Structural relationships of biotites. (**a**) Volume of M1 site (Å^3) vs. volume of M2 site (Å^3) (standard deviation: $\sigma < 0.01$); (**b**) Mean <M2-O3> length (Å) ($\sigma \le 0.003$) vs. $^{[6]}Al^{3+}$ content (apfu); (**c**) Octahedral thickness (Å) ($\sigma \le 0.004$) vs. $^{[6]}$Al content (apfu). Symbols: triangle up-pointing = biotites from Sardinia (Italy) peraluminous granites; triangle down-pointing = biotites-1*M* from Northern Victoria Land (Antarctica) peraluminous granites; square = biotite-2M_1 from Northern Victoria Land (Antarctica) peraluminous granites; diamond = biotites from Valle del Cervo (Northwestern Italy) plutonic complex (Brigatti and Davoli 1990); hexagon = biotites from Warburton granodiorite, Lachlan Fold Belt, Australia (Brigatti et al. 1998b).

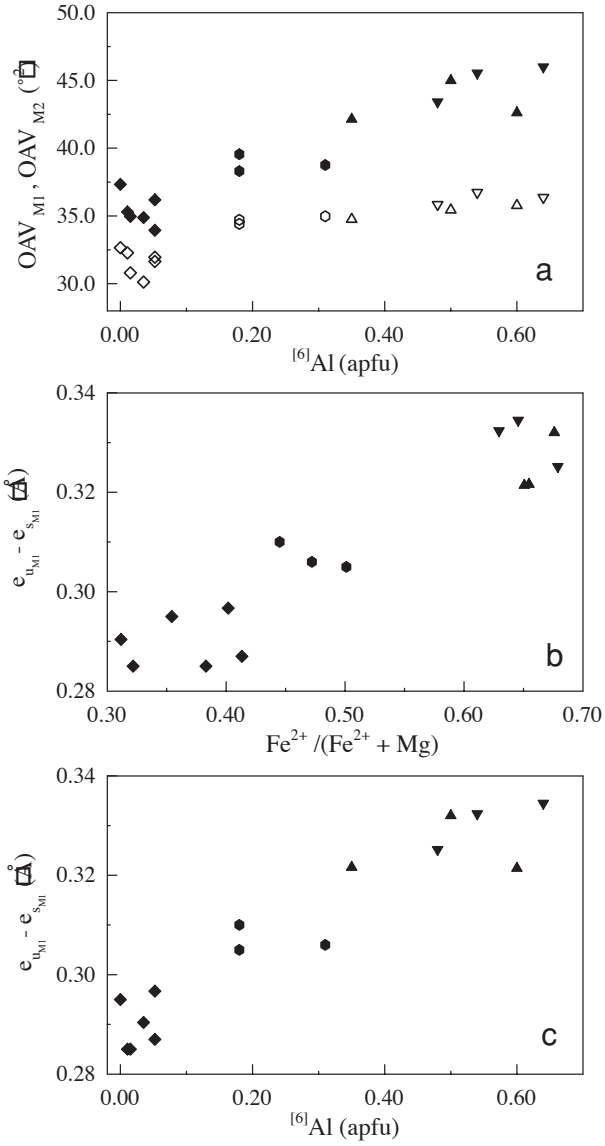

FIGURE 5. Structural relationships of biotites. See table for definitions. (**a**) OAV (°²) of M1 site (filled symbols) compared with OAV of M2 site (open symbols) vs. [6]Al content (apfu); (**b**) e_{uM1}–e_{sM1} (Å) vs. Fe/(Fe + Mg); (c) e_{uM1}–e_{sM1} (Å) (standard deviation: $\sigma \leq 0.004$) vs. [6]Al. Symbols: triangle up-pointing (both open and filled) = biotites from Sardinia peraluminous granites; triangle down-pointing (both open and filled) = biotites-1*M* from Northern Victoria Land peraluminous granites; square = biotite-2M_1 from Northern Victoria Land peraluminous granites; diamond (both open and filled) = biotites from Valle del Cervo (Northwestern Italy) plutonic complex (Brigatti and Davoli 1990); hexagon (both open and filled) = biotites from Warburton granodiorite, Lachlan Fold Belt (Brigatti et al. 1998 b).

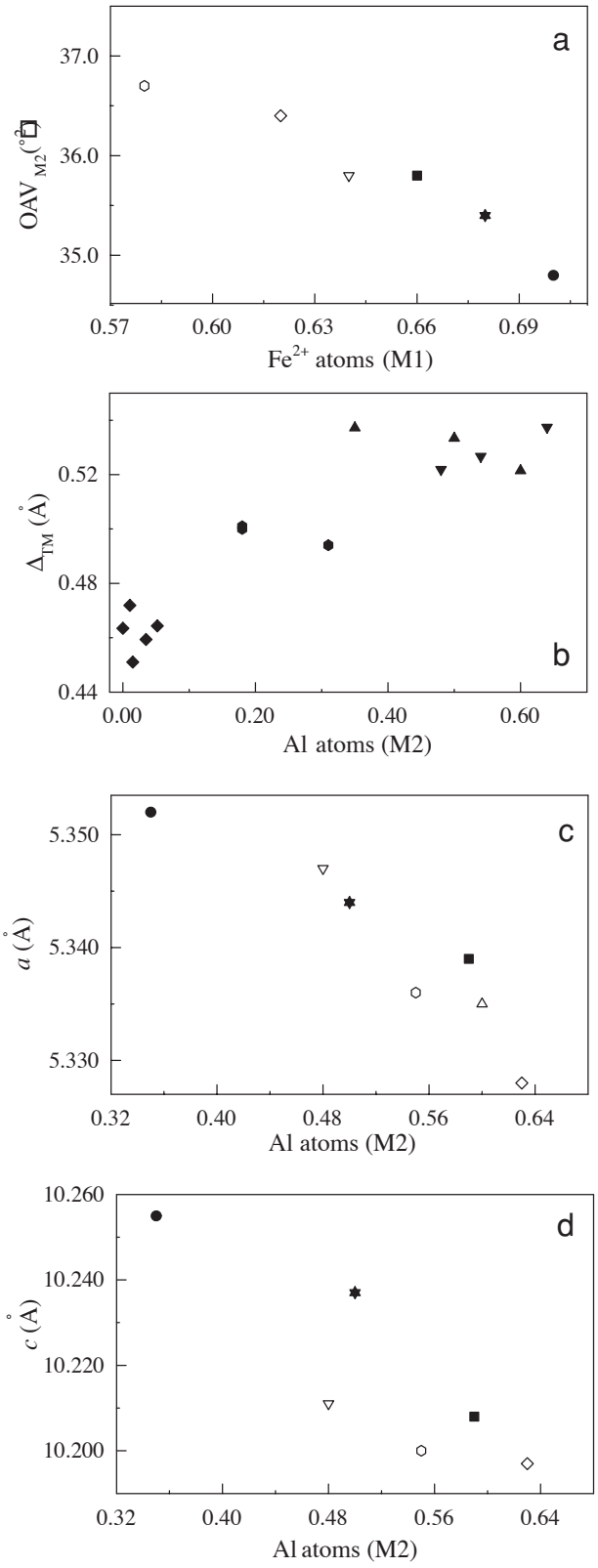

FIGURE 6. (**a**) M2 site angle variance [OAV_{M2} (°²)] vs. Fe^{2+}_{M1}; (**b**) dimensional misfit (Å) between tetrahedral and octahedral sheets vs. Al content in M2 sites; (**c**) unit-cell parameter *a* (Å) ($\sigma \leq 0.003$) vs. Al content in M2 sites; (**d**) unit-cell parameter *c*(Å) ($\sigma \leq 0.004$) vs. Al content in M2 sites of the biotite-1*M* crystals. Symbols: circle = A4 sample, square = GFS15a sample, star = H87 sample; diamond = CC1 sample, down-pointing triangle = C3-31 sample, hexagon = B1 sample, up-pointing triangle = C6c sample.

enlarges and the distortion is less stressed (Fig. 6a). The different composition and degree of ordering of octahedral sites creates differences in the bond valence arrangement on O3 and O4 sites (Lee and Guggenheim 1981). Because O3 atoms are the bridging atoms of the tetrahedra, it is expected that the octahedral variation affects strongly the configuration of the tetrahedral sheet. The plot of Δ_{TM} values vs. $^{[6]}$Al apfu in Figure 6b confirms a significant increase in dimensional misfit between tetrahedral and octahedral sheets in $^{[6]}$Al-rich crystals.

The extent of tetrahedral substitution, as determined by electron microprobe analysis, is always lower than 35%. The tetrahedron is quite regular, as measured by the tetrahedral quadratic elongation (TQE ≤ 1.0002), and angle variance [TAV ≤ 0.8(°^{2})] and slightly elongated (110.1 ≤ τ ≤ 110.2°). The mean tetrahedral bond lengths range from 1.657 to 1.665 Å and do not correlate with $^{[6]}$Al. Furthermore, the <T-O> distances in $^{[6]}$Al-rich biotites are close to the distances found in biotites from plutonic environments previously reported.

The lengths of unit-cell edges of Al-rich biotites all decrease with Al content in M2 (Figs. 6c and 6d) and increase with Fe content in M1. These results are expected owing to the variation of <M2-O> bond lengths and many other geometrical parameters previously discussed.

Biotite-2M$_1$. The tetrahedral bond lengths reflect Al-Si disorder, and both tetrahedra show similar distortion parameters, the only difference being that tetrahedral T2 cations are slightly displaced from the center of the polyhedron with respect to the T1 site (BLD_{T1} = 0.197; BLD_{T2} = 0.345). As in biotites-1*M*, the composition of the octahedral sheet is characterized by a high Al content (0.60 apfu), and is similar to 1*M* polytype, <M2-O> being shorter than <M1-O> and the distortion of both M1 and M2 sites appearing to be correlated with the $^{[6]}$Al content. The octahedral sheet thickness and the dimensional misfit agree well with the relationships given in Figures 4c and 6b, suggesting that the layer geometry depends on the $^{[6]}$Al content. The comparison with biotites 2M_1 from other plutons (Bigi and Brigatti 1994) show a decrease of 2.2% in M2 site volume which is related to the distortion increase of both octahedral sites (Table 9).

Coexisting muscovites. Dioctahedral micas coexisting with biotites in the peraluminous granites studied are Mg-, Fe-bearing muscovites-2M_1 (Brigatti et al. 1998a). Actually, compared with the end-member composition, they exhibit Fe and Mg and small Ti and Mn substitutions for octahedral Al. Figures 2e–2h show that exchange vectors balancing the $^{[6]}$Al substitution mostly agree with the phengitic operator (Fig. 2e).

Structure refinement verifies that there is no apparent ordering in tetrahedral sites; <T1-O> and <T2-O> distances are equivalent and, except for the ordered vacancy in the trans-M1 site, no other octahedral ordering between M2 sites was found. The mean electron count for the M2 site is greater than 13 e$^-$, indicating that cations heavier than Al occupy the M2 octahedral site, and are closely connected with phengitic substitution. Besides, all the refined crystals show residual areas of positive electron densities close to the M1 site position, indicating a partial M1 occupation.

The presence of Mg and Fe in octahedral coordination increases the dimensions of M2 sites with respect to the end member, with a consequent increase in the thickness and in the lateral dimension of the octahedral sheet (Fig. 7a). Furthermore, the excess of electron density at the M1 position reduces the dimensions of the vacant cavity. The tetrahedra have less out-of plane tilt to fit apical O atoms with the octahedral sheet and, consequently, α decreases and the coplanarity of the basal tetrahedral O atoms is improved. Figure 7b confirms that the reduced differences between M1 and M2 site distortion principally affect the interlayer cation coordination.

Relationships among biotites, phengitic muscovites, and host rock. Replacement of Mg and Fe by Al in biotite induces major changes in the geometry of the M2 polyhedron, which reduces <M2-O> bond distances as the Al content increases and accentuates the M1 octahedral site distortion. Both Fe and Mg are distributed over the M1 and M2 sites; however, Fe shows a small but consistent preference for M1. The mean intracrystalline partition coefficient $D^{M1/M2}$ [$D^{M1/M2} = (Fe/Mg_{M1})/(Fe/Mg)_{M2}$] varies from 0.73 to 4.80 and roughly decreases with increasing occupancy of M2 by high charge cations (i.e., Al

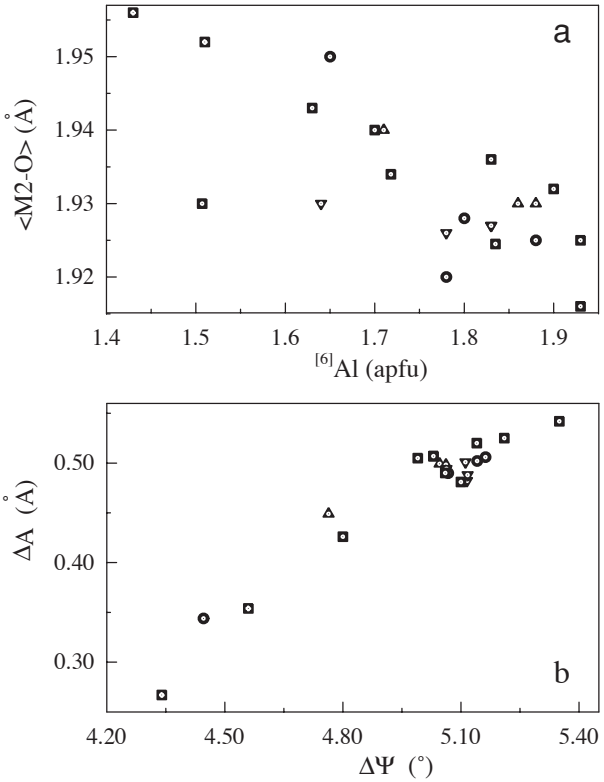

FIGURE 7. Structural relationships of muscovites. (**a**) <M2-O> length (Å) vs. $^{[6]}$Al content (apfu); (**b**) difference between outer and inner interlayer cation coordination $\Delta A = <A\text{-}O>_{outer} - <A\text{-}O>_{inner}$ (Å) vs. difference between the flattening of the two octahedral cavities $\Delta\Psi = \Psi_{M1} - \Psi_{M2}$ (°). Symbols: up-pointing triangle = muscovites coexisting with studied biotites from Sardinia (Brigatti et al. 1998a); down-pointing triangle = muscovites coexisting with studied biotites from Northern Victoria Land (Brigatti et al. 1998 a); circle = muscovites from literature (Birle and Tettenhorst 1968; Güven 1971; Rothbauer 1971; Richardson and Richardson 1982; Rule and Bailey 1985; Knurr and Bailey 1986; Guggenheim et al. 1987; Catti et al. 1989; Brigatti et al. 1998a).

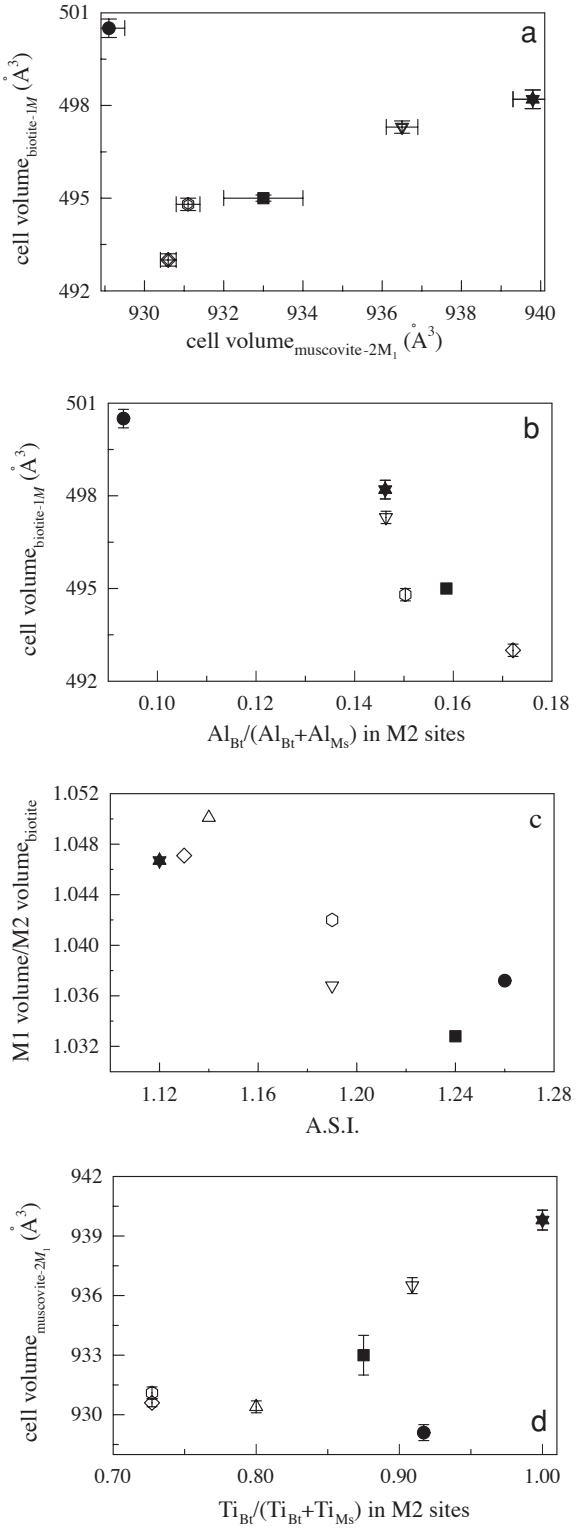

FIGURE 8. (**a**) Cell volume (Å^3) of biotite-1*M* crystals vs. cell volume (Å^3) of muscovite-2M_1 crystals; (**b**) biotite cell volume (Å^3) vs. the $D(Al)_{M2}^{Bt/Ms}$ partition coefficients ($Al_{M2}^{Bt}/Al_{M2}^{Ms}$); (**c**) ratio between M1 and M2 volumes in biotite vs. Al saturation index (A.S.I) of the host rock; (**d**) muscovite-2M_1 cell volume (Å^3) vs. $Ti_{Bt}/(Ti_{Bt} + Ti_{Ms})$ in M2 sites. Symbols as in Figure 6.

and Ti). By comparing our data with those reported previously for biotite crystals from metaluminous plutons, the ordering parameter $Q_{M1,M2} = |(<M1\text{-}O> - <M2\text{-}O>)| /1/2(<M1\text{-}O> + <M2\text{-}O>)$ (Carpenter et al. 1990) is systematically higher ($1.0\cdot10^{-2} \le Q_{M1,M2} \le 1.7\cdot10^{-2}$) than that obtained for biotite crystals from Valle del Cervo ($0.4\cdot10^{-2} \le Q_{M1,M2} \le 0.8\cdot10^{-2}$) and from Warburton granodiorite complexes ($0.05\cdot10^{-2} \le Q_{M1,M2} \le 0.8\cdot10^{-2}$). The greater ordering in biotite crystals from peraluminous granites can be attributed either to crystal chemical constraints (i.e., small high-charged cations prefer octahedra with OH in cis-orientation, Bailey 1984) or to the intensive variables acting during crystallization.

The refinements of muscovite crystals indicate the typical dioctahedral ordering pattern with the vacancy ordered in the trans-M1 site. Elements heavier than Al occupy M2, which agrees with the amount of phengitic substitution determined by chemical analysis. Residual electron densities at M1, which could be related to octahedral ordering, are small and inconsistent. As the phengitic component increases, the M2 site volume enlarges, the M1 vacant cavity contracts and the difference in dimensions between M1 and M2 decreases. Therefore, there appears to be an inverse relationship between phengitic substitution and metrical order.

The <T1-O> distances are slightly longer than both <T1-O> and <T2-O> distances in muscovite for all biotite crystals (Table 6, Brigatti et al. 1998a). The average <T-O> distance for biotite crystals is 1.660(3), whereas in muscovites it is 1.646(9) and 1.645(6) for <T1-O> and <T2-O>, respectively. The lengthening of <T-O> bond distance in biotite could be attributed both to the $^{[4]}Al$-$^{[6]}Al$ coupled substitution and to the increased bond valence of the M2-O3 bond. In contrast, in muscovite, changes in the content of phengitic substitution are accompanied by shortening of the mean tetrahedral bond-lengths and the lengthening of <M2-O> (Brigatti et al. 1998a).

Comparison of the structural features of these coexisting micas provides evidence to confirm the equilibrium crystallization. Excluding sample A4, the unit-cell volumes of coexisting micas increase in a similar way (Fig. 8a). A plausible explanation for the anomalous behavior of sample A4 could be a lack of equilibrium during subsolidus compositional changes. Figure 8b displays the variation of the biotite cell volume with Al partition coefficient $D(Al)_{M2}^{Bt/Ms}$ (Tables 3 and 10, Brigatti et al. 1998a) and Figure 8c shows the effect of the rock composition, expressed as the Al saturation index (A.S.I. parameter, Table 1), on octahedral M site volumes. The M site and unit cell volumes of both micas decrease with the decrease of rock Al content and this is a reflection of the influence of melt composition on both crystals. Finally, the behavior of the Ti component is opposed to that of Al showing an increase of M2 site and unit cell volumes in coexisting micas with $Ti_{Bt}/(Ti_{Bt} + Ti_{Ms})$ (Fig. 8d) and this, according to Patiño Douce (1993), is a reflection of the influence of temperature during mica growth.

In summary the structure of coexisting micas in peraluminous granitoids appears to be a good indicator of chemical events during crystallization. Besides, their crystal chemistry can be very useful for understanding fluid activity, temperature, and pressure during mica growth. These are goals for forthcoming experimental studies.

ACKNOWLEDGMENTS

It is a pleasure to thank M. Mellini and C. Viti for their assistance in TEM analyses that although not reported were very useful to confirm stacking sequence relationships between coexisting micas. Constructive reviews were provided by D.M. Jenkins, A. Patinio Douce, and D. Peacor. This work was carried out with the support of MURST (projects: PNRA and "Modellizzazione della composizione petrografica e geochimica della crosta continentale in alcune aree tipo italiane") and of Italian CNR. The CNR and CIGS (Modena University) were acknowledged for financing the Electron Microprobe and the XRD Laboratory of the University of Modena, respectively.

REFERENCES CITED

Bailey, S.W. (1984) Crystal chemistry of the true micas. In Mineralogical Society of America Reviews in Mineralogy, 13, 13–60.

Beattie, P., Drake, M., Jones, J., Leeman, W., Longhi, J., McKay, G., Nielsen, R., Palme, H., Shaw, D., Takahashi, E., and Watson, B. (1993) Terminology for trace-element partitioning. Geochimica et Cosmochimica Acta, 57, 1605–1606.

Biagini, R., Di Vincenzo, G., and Ghezzo, C. (1991) Petrology and Geochemistry of peraluminous granitoids from Priestley and Aviator glacier region, Northern Victoria Land, Antarctica. Memorie della Società Geologica Italiana, 46, 205–230.

Bigi, S. and Brigatti, M.F. (1994) Crystal chemistry and microstructures of plutonic biotite. American Mineralogist, 79, 63–72.

Birle, J.D. and Tettenhorst, R. (1968) Refined muscovite structure. Mineralogical Magazine, 36, 883–886.

Brigatti, M.F. and Davoli, P. (1990) Crystal structure refinement of 1M plutonic biotites. American Mineralogist, 75, 305–313.

Brigatti, M.F., Frigieri, P., and Poppi, L. (1998a) Crystal chemistry of Mg-, Fe^{2+}–bearing muscovites-$2M_1$. American Mineralogist., 83, 775–785.

Brigatti, M.F., Lugli, C., Poppi, L., and Elburg, M. (1998b) Crystal chemistry of biotites from mafic enclaves in the Warburton granodiorite, Lachlan Fold Belt (Australia). European Journal of Mineralogy, 10, 855–864

Busing, W.R., Martin, K.O., and Levi, H.S, (1962) ORFLS, a Fortran crystallographic least-squares program. U. S. National Technical Information Section, ORNL–TM–305.

Carpenter, M.A., Domeneghetti, M.C., and Tazzoli, V. (1990) Application of Landau theory to cation ordering in omphacite. I : Equilibrium behaviour. European Journal of Mineralogy, 2, 7–18.

Catti, M., Ferraris, G., and Ivaldi, G. (1989) Thermal strain analysis in the crystal structure of muscovite at 700 °C. European Journal of Mineralogy, 1, 625–632.

De Albuquerque, C.A.R. (1975) Partition of trace elements in co-existing biotite, muscovite and potassium feldspar of granitic rocks, Northen Portugal. Chemical Geology, 16, 89–108.

Di Vincenzo, G., Ghezzo, C., and Tonarini, S. (1994) Geochemistry and Rb-Sr geochronology of the Hercynian peraluminous Sos Canales pluton (central Sardinia, Italy). Comptes Rendu de l'Académie des Sciences Paris, 319, série II, 783–790.

Di Vincenzo, G., Andriessen, P.A.M., and Ghezzo, C. (1996) Evidence of Two Different Components in a Hercynian Peraluminous Cordierite-bearing Granite: the San Basilio Intrusion (Central Sardinia, Italy). Journal of Petrology, 37, 1175–1206.

Donnay, G., Morimoto, N., Takeda, H., and Donnay, D.H. (1964) Trioctahedral one-layer micas: 1. Crystal structure of a synthetic iron mica. Acta Crystallographica, 17, 1369–1373.

Donovan, J.J. (1995) PROBE: PC-based data acquisition and processing for electron microprobes. Advanced Microbeam, 4217 King Graves Rd., Vienna, Ohio, 44473.

Foley, S.F. (1989) Experimental constraints on phlogopite chemistry in lamproites: 2. The effect of pressure-temperature variations. European Journal of Mineralogy, 2, 327–341.

Guggenheim, S., Chang, Y.H., and Koster van Groos, A.F. (1987) Muscovite dehydroxylation: High-temperature studies. American Mineralogist, 72, 537–550.

Guidotti, C.V. (1978) Compositional variation of muscovite in medium- to high-grade metapelites of northwestern Maine. American Mineralogist, 63, 878–884.

——(1984) Micas in metamorphic rocks. In Mineralogical Society of America Reviews in Mineralogy, 13, 357–468.

Guidotti, C.V., Cheney, J.T., and Guggenheim, S. (1977) Distributiom of titanium between coexisting muscovite and biotite in pelitic schists from northwestern Maine. American Mineralogist, 62, 438–448.

Guidotti, C.V., Sassi, F.P., and Blencoe, J.G. (1989) Compositional controls on the *a* and *b* cell dimentions of $2M_1$ muscovite. European Journal of Mineralogy, 1, 71–84.

Guidotti, C.V., Yates, M.G., Dyar, M.D., and Taylor, M.E. (1994) Petrogenetic implications of the Fe^{3+} content of muscovite in pelitic schists. American Mineralogist, 79, 793–795.

Güven, N. (1971) The crystal structures of $2M_1$ phengite and $2M_1$ muscovite. Zeitschrift für Kristallographie, 134, 196–212.

Hazen, R.M. and Burnham, C.W. (1973) The crystal structures of one-layer phlogopite and annite. American Mineralogist, 58, 889–900.

Hoisch, T.D. (1989) A muscovite-biotite geothermometer. American Mineralogist, 74, 565–572.

Icenhower, J. and London, D. (1995) An experimental study of element partitioning among biotite, muscovite, and coexisting peraluminous silicic melt at 200 MPa (H_2O). American Mineralogist, 80, 1229–1251.

Joswig,W. (1972) Neutronenbeugungsmessungen an einem 1*M*-phlogopit. Neues Jahrbuch für Mineralogie Monatshefte, 1–11.

Lee, J.H. and Guggenheim, S. (1981) Single crystal X-ray refinement of pyrophyllite-1*Tc*. American Mineralogist, 66, 350–357.

Knurr, R.A. and Bailey, S.W. (1986) Refinement of Mn-substituted muscovite and phlogopite.Clays and Clay Minerals, 34, 7–16.

Meyrowitz, R. (1970) New semimicroprocedure for determination of ferrous iron in refractory silicate minerals using a sodium metafluoborate decomposition. Analytical Chemistry, 42, 1110–1113.

Miller, C.F. (1985) Are strongly peraluminous magmas derived from pelitic sedimentary source? Journal of Geology, 93, 673–689.

Miller, C.F., Stoddard, E.F., Bradfish, L.J., and Dollase, W.A. (1981) Composition of plutonic muscovite: genetic implications. Canadian Mineralogist, 19, 25–34.

Monier, G. and Robert, J.L. (1986) Titanium in muscovites from two mica granites: substitutional mechanism and partition with coexisting biotites. Neues Jahrbuch für Mineralogie Abhandlungen, 153, 147–161.

Neiva, A.M.R., Neiva, J.M., and Parry, S.J. (1987) Geochemistry of the granitic rocks and their minerals from Serra da Estrela, Central Portugal. Geochimica et Cosmochimica Acta, 51, 439–454.

Patiño Douce, A.E. (1993) Titanium substitution in biotite: an empirical model with applications to thermometry, O_2 and H_2O barometries, and consequences for biotite stability. Chemical Geology, 108, 133–162.

Patiño Douce, A.E. and Johnston, A.D. (1991) Phase equilibria and melt productivity in the pelitic system: implication for the origin of peraluminous granitoids and aluminous granulites. Contributions to Mineralogy and Petrology, 107, 202–218.

Patiño Douce, A.E., Johnston, A.D., and Rice, J.M. (1993) Octahedral excess mixing properties in biotite: a working model with applications to geobarometry and geothermometry. American Mineralogist, 78, 113–131.

Pitcher, W.S. (1988). Andean batholiths and marginal basins. Rendiconti della Società Italiana di Mineralogia e Petrologia, 43-3, 275–280.

Renner, B. and Lehmann, G. (1986) Correlation of angular and bond length distortion in TO_4 units in crystals. Zeitschrift für Kristallographie, 175, 43–59.

Richardson, S.M. and Richardson, J.W. Jr. (1982) Crystal structure of a pink muscovite from Archer's Post, Kenya: implications for reverse pleochroism in dioctahedral micas. American Mineralogist, 67, 69–75.

Robinson, K., Gibbs, G.V., and Ribbe, P.H. (1971) Quadratic elongation: A quantitative measure of distortion in coordination polyhedra. Science, 172, 567–570.

Rothbauer, Von R. (1971) Untersuchung eines $2M_1$-Muskovits mit Neutronenstrahlen. Neues Jahrbuch für Mineralogie Monatshefte, 143–154.

Rule, A.C. and Bailey, S.W. (1985) Refinement of the crystal structure of phengite-$2M_1$. Clays and Clay Minerals, 33, 403–409.

Siemens (1996) XSCANS: X-ray Single Crystal Analysis System-Technical reference. Siemens instruments.

Speer, J.A. (1984) Micas in Igneous Rocks. In Mineralogical Society of America Reviews in Mineralogy, 13, 299–356.

Toraya, H. (1981) Distortions of octahedra and octahedral sheets in 1*M* micas and the relation to their stability. Zeitschrift für Kristallographie, 157, 173–190.

Tracy, R.J. (1978) High-grade metamorphic reactions and partial melting in pelitic schist, west-central Massachusetts. American Journal of Science, 278, 150–178.

Ungaretti, L. (1980) Recent developments in X-ray crystal diffractometry applied to the crystal chemical study of amphiboles. Godisnjac Iugoslavenskog Centraza Kristalograiju, 15, 29–65.

Ungaretti, L., Lombardo, B., Domeneghetti, M.C., and Rossi, G. (1983) Crystal Chemical evolution of amphiboles from eclogitised rocks of the Sesia-Lanzo Zone, Italian western Alps. Bulletin de Minéralogie, 106, 645–672.

Weiss, Z., Rieder, M., Chmielová, M., and Krajícek, J. (1985) Geometry of the octahedral coordination in micas: a review of refined structures. American Mineralogist, 70, 747–757.

Weiss, Z., Rieder, M., and Chmielová, M. (1992) Deformation of coordination polyhedra and their sheets in phyllosilicates. European Journal of Mineralogy, 4, 665–682.

White, A.J.R. and Chappell, B.W. (1983) Granitoids types and their distribution in the Lachlan Fold Belt. Southeastern Australia. Geological Society of America Memoir, 159, 21–33.

MANUSCRIPT RECEIVED FEBRUARY 24, 1999
MANUSCRIPT ACCEPTED OCTOBER 26, 1999
PAPER HANDLED BY DAVID M. JENKINS